Journal of Structural Geology 71 (2015) 58–70

Contents lists available at ScienceDirect

Journal of Structural Geology

journal homepage: www.elsevier.com/locate/jsg

Fabric development during exhumation from ultrahigh-pressure in an eclogite-bearing shear zone, Western Gneiss Region, Norway

Roxanne N. Renedo [a, *], William O. Nachlas [a], Donna L. Whitney [a], Christian Teyssier [a], Sandra Piazolo [b], Stacia M. Gordon [c], Haakon Fossen [d]

[a] Department of Earth Sciences, University of Minnesota, Minneapolis, MN 55455, USA
[b] ARC Centre of Excellence for Core to Crust Fluid Systems and GEMOC, Department of Earth and Planetary Sciences, Macquarie University, NSW 2109, Australia
[c] Department of Geological Sciences, University of Nevada, Reno, NV 89557, USA
[d] Department of Earth Science, University of Bergen, 5007 Bergen, Norway

ARTICLE INFO

Article history:
Available online 18 September 2014

Keywords:
Western Gneiss Region
Ultrahigh-pressure
Ti-in-quartz thermobarometry
Electron backscatter diffraction
Omphacite CPO
Quartz CPO

ABSTRACT

Petrofabrics and trace-element thermobarometry of deformed quartzofeldspathic gneiss and associated coesite-bearing eclogite in the Salt Mylonite Zone (Western Gneiss Region, Norway) document a pressure–temperature–deformation path from ultrahigh-pressure to amphibolite-facies conditions. The Salt mylonite zone is dominated by quartzofeldspathic gneiss with a strong foliation and lineation. Coesite-bearing eclogite within the shear zone contains a foliation and lineation (defined by elongate omphacite) consistent with that of the host gneiss, suggesting that gneiss and eclogite were deformed in the same kinematic framework. In eclogite, omphacite preserves LS- to L-type crystallographic preferred orientation, and quartz preserves prism <c> fabrics that developed in quartz near coesite–quartz transition conditions. The quartzofeldspathic gneiss in the mylonite zone records prism and rhomb <a> slip in quartz and reverse zoning in plagioclase (higher Ca rims) consistent with re-equilibration during decompression. The Ti concentration in quartz in gneiss is higher than that in quartz in eclogite, suggesting that quartz recrystallized at a lower pressure in the gneiss. Ti-in-quartz thermobarometry of rutile-bearing eclogite and titanite-bearing gneiss indicates equilibration at $T > 750$ °C and $T < 650$ °C, respectively. This mylonite zone preserves a discontinuous record of fabric development from incipient stages of exhumation of ultrahigh-pressure rocks to crustal conditions.

1. Introduction

Numerous (>20) ultrahigh-pressure (UHP) terranes have been identified globally (Zheng, 2012); the abundance of these terranes shows that the exhumation of deeply-subducted continental crust is a common consequence of continental collision. UHP terranes record chemical and physical processes that occur during continental collision, subduction, and exhumation. An unresolved question concerns the exhumation mechanism(s) of UHP terranes, a query that may be approached, in part, by documenting the conditions and mechanisms of deformation in shear zones that were active from mantle depths (high pressure, HP, and possibly UHP conditions) to lower-to mid-crustal depths.

The Western Gneiss Region (WGR) is one of the largest and best-exposed UHP terranes. Here, evidence of HP and UHP metamorphism is typically preserved in lenses (pods) of eclogite dispersed in highly deformed quartzofeldspathic gneiss (e.g., Smith, 1984; Wain, 1997; Carswell et al., 2003a,b; Hacker et al., 2010). Discrete shear zones in the quartzofeldspathic gneiss are documented throughout the WGR. In some of these shear zones, both gneiss and eclogite underwent significant deformation and now record a range of pressure–temperature–deformation (P–T–d) conditions from prior to exhumation to emplacement at crustal levels.

We have investigated in detail a ductile shear zone that consists of quartzofeldspathic gneiss that hosts a strongly deformed UHP (coesite-bearing) eclogite layer: the Salt mylonite zone (SMZ; Figs. 1 and 2a). In this paper, we document and discuss the conditions under which mesoscopic structures and microfabrics developed in eclogite and gneiss in the SMZ. Ti-in-quartz thermobarometry and

* Corresponding author.
E-mail address: rened001@umn.edu (R.N. Renedo).

http://dx.doi.org/10.1016/j.jsg.2014.09.012
0191-8141/

microfabric analysis are used to explore deformation conditions and mechanisms as a function of pressure (P). We show that eclogite fabrics likely formed under HP conditions ($P > 2$ GPa) following decompression from UHP conditions, and that fabrics in the quartzofeldspathic gneiss developed over a wide range of P and temperature (T) conditions during decompression to crustal levels ($P < 1$ GPa).

2. Overview of the Western Gneiss Region

The WGR of Norway (Fig. 1) is a large UHP terrane that covers 50,000 km^2; at least 5% of the WGR preserves UHP conditions, primarily in eclogite lenses hosted in gneiss (e.g., Hacker et al., 2010). The WGR formed during the Caledonian orogeny as a result of the subduction of Baltica beneath Laurentia (ca. 425–400 Ma) during which UHP conditions were attained (Andersen et al., 1991, 1998; Carswell et al., 2003a; Root et al., 2004). Exhumation of the terrane to amphibolite-facies conditions was largely achieved by ca. 390–380 Ma (Andersen et al., 1998; Hacker, 2007; Young et al., 2011).

The WGR is dominated by strongly deformed, tonalitic to granodioritic, migmatitic gneiss (e.g., Hacker et al., 2010). The gneiss preserves primarily amphibolite-facies assemblages that may represent re-equilibration during exhumation and overprinting of (U)HP assemblages and textures (Griffin and Brueckner, 1985; Wain, 1997; Terry and Robinson, 2003; Labrousse et al., 2004). Moreover, the gneiss contains metamorphosed mafic (eclogite, amphibolite) and ultramafic rocks (peridotites) that form centimeter to kilometer scale layers and lenses.

UHP metamorphism in the WGR is identified by the presence of index minerals including coesite and microdiamond (e.g., Smith, 1984; Griffin and Brueckner, 1985; Wain, 1997; Wain et al., 2000; Cuthbert et al., 2000; Butler et al., 2012; Smith and Godard, 2013). Coesite and polycrystalline quartz (Pcq, interpreted as a pseudomorph after coesite; Smyth, 1977) are commonly found as inclusions in garnet and clinopyroxene in eclogite (e.g., Smith, 1984) and less commonly as inclusions in garnet and clinozoisite in gneiss (Wain, 1997). Microdiamond has also been reported from garnet–kyanite gneiss (Dobrzhinetskaya et al., 1995) and metamorphosed ultramafic rocks (Vrijmoed et al., 2006).

The occurrence of UHP minerals in the WGR defines three UHP domains. From south to north these are the Nordfjord, Sørøyane, and Nordøyane UHP domains (Fig. 1). Rocks in the intervening regions record HP (but not UHP) conditions (Wain, 1997; Root et al., 2005; Hacker, 2007). Previous research suggests a general increase of P and T to the northwest in the WGR (e.g., Hacker et al., 2010), with the lowest peak conditions preserved in the Nordfjord UHP domain (700–800 °C and ~2.8–3.0 GPa; Wain, 1997; Johnston et al., 2007) and the highest peak conditions preserved in the Nordøyane UHP domain (>800 °C and 3.5–4.0 GPa; Terry et al., 2000). This interpretation is complicated, however, by the

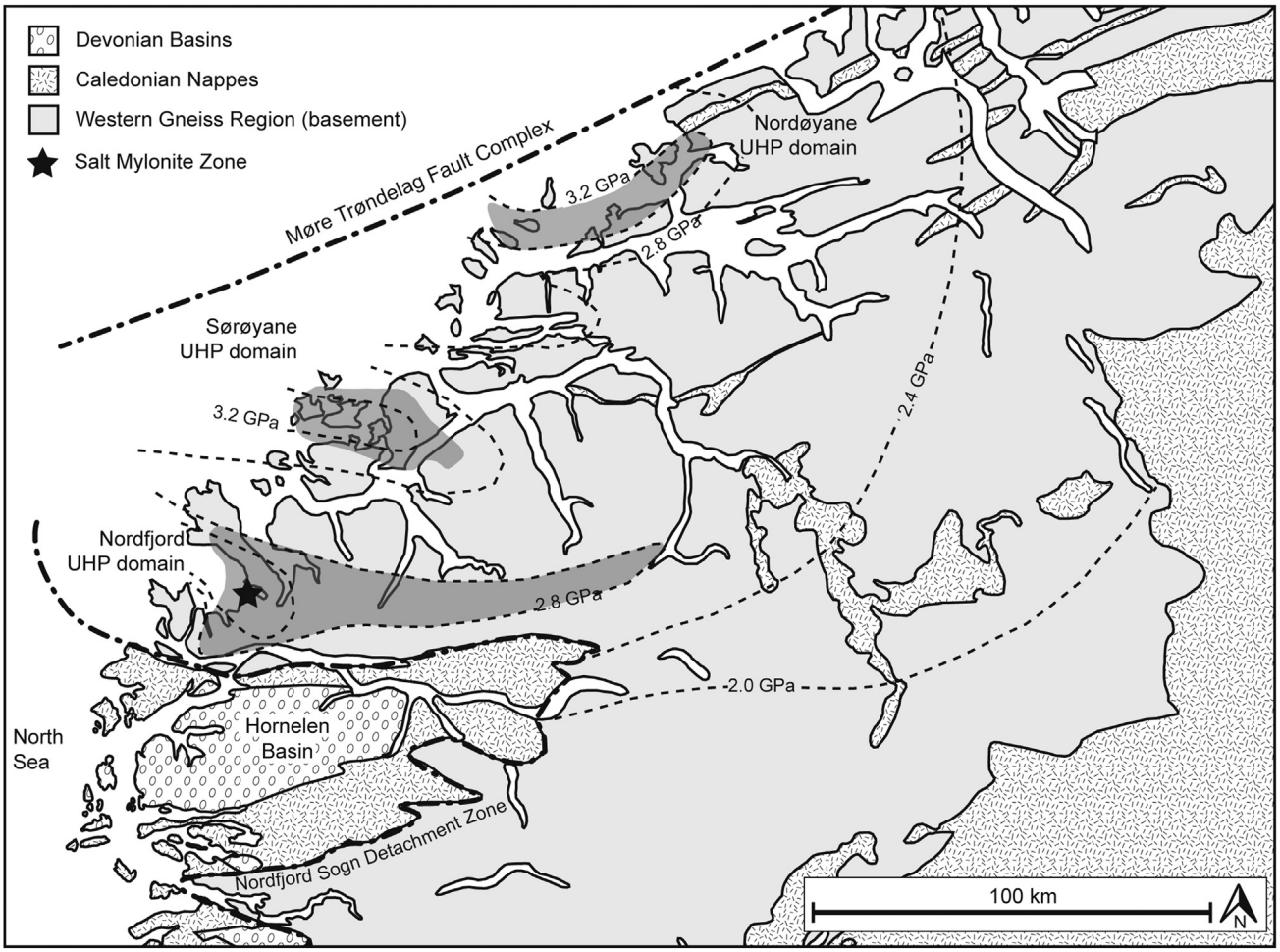

Fig. 1. Map of the WGR, Norway. The HP (light gray) and UHP (dark gray) WGR is bound by the Nordfjord Sogn detachment zone to the south and west and by the Møre-Trondelag fault complex to the north. The Nordfjord Sogn detachment zone separates the basement from the overlying allochthonous nappes and Devonian basins (i.e., the Hornelen basin). The three UHP domains are exposed along the western coast, from south to north they are: the Nordfjord, the Sørøyane, and the Nordøyane UHP domains. Isobars (from Hacker et al., 2010 and references therein) are shown on the map; these data suggest a general P (and T) increase to the NW. The SMZ is located in the Nordfjord UHP domain (black star).

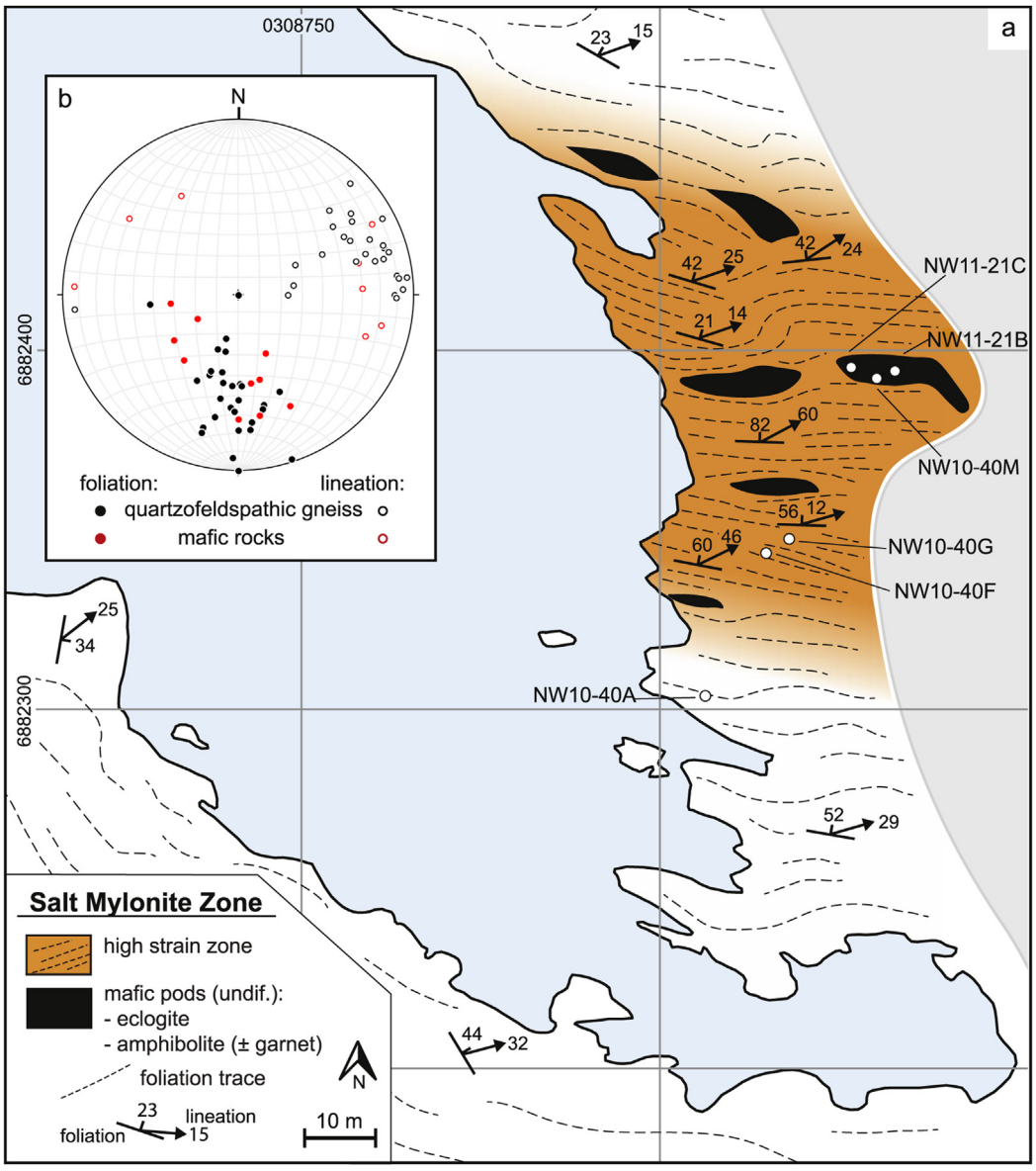

Fig. 2. (a) Map of the SMZ (highlighted in orange) with quartzofeldspathic gneiss structural measurements and sample locations. Mafic rocks (eclogite and amphibolite, black) are contained within the quartzofeldspathic host gneiss. (b) Stereonet of structural measurements from the SMZ. The foliation of the quartzofeldspathic gneiss (poles to planes represented by black, filled circles) and mafic rocks (eclogite and amphibolite, poles to planes represented by red filled circles) are similarly oriented, whereas gneiss and mafic rocks lineations (hollow circles of the same color) are slightly more variable. (For interpretation of the references to color in this figure legend, the reader is referred to the web version of this article.)

recent discovery of microdiamond of unknown age in eclogite from the Nordfjord UHP domain (Smith and Godard, 2013), indicating minimum pressures of ~3.5 GPa for at least part of this domain. If this diamond-forming metamorphism is Caledonian, then this, along with the coexistence of HP and UHP eclogite (Wain, 1997; Wain et al., 2000), is further evidence of heterogeneity in WGR *P–T* conditions and/or in the preservation of peak metamorphic assemblages.

The structures of the WGR, from the scale of the orogen to mesoscopic fabrics, suggest that exhumation was accommodated by oblique extension. At the largest scale, this is indicated by the interplay of the Nordfjord Sogn detachment zone and the Møre-Trondelag fault complex, the normal and strike slip fault zones, respectively, that bound the WGR (Norton, 1986, 1987; Braathen et al., 2000). The interplay of these fault zones resulted in the development of corrugated detachments (Krabbendam and Dewey, 1998). In this regard, the UHP domains have been interpreted as possible transtensional antiforms (Krabbendam and Dewey, 1998; Fossen et al., 2013). Mineral and stretching lineations are oblique to the trend of the orogen (Fossen, 2010), and constrictional fabrics have been documented in rocks throughout the WGR (e.g., Barth et al., 2010). These features are consistent with oblique extension, at least at amphibolite-facies conditions (Krabbendam and Dewey, 1998).

3. The Salt mylonite zone

The SMZ (Fig. 2a) is a 60 m wide zone of localized ductile deformation in quartzofeldspathic gneiss (referred to as the 'country-rock gneiss'). The country-rock gneiss is medium grained, contains layer-parallel leucosomes, preserves a well-developed foliation with variable orientations and a pervasive east plunging

mineral lineation, and contains variably retrogressed eclogite pods and amphibolite (±garnet) layers and lenses (m-scale). In comparison, within the SMZ, the quartzofeldspathic gneiss is characterized by 'stripes' of fine-scale compositional layering. The striped gneiss is finer-grained, displays a strong, planar east–west trending foliation with a consistent steep to moderate dip to the north (Fig. 3a), and a well-defined mineral lineation with a shallow to moderate plunge to the east. Although overall fine-grained, some gneiss layers within the SMZ contain large (up to 1 cm) potassium feldspar porphyroclasts with recrystallized tails that display σ and

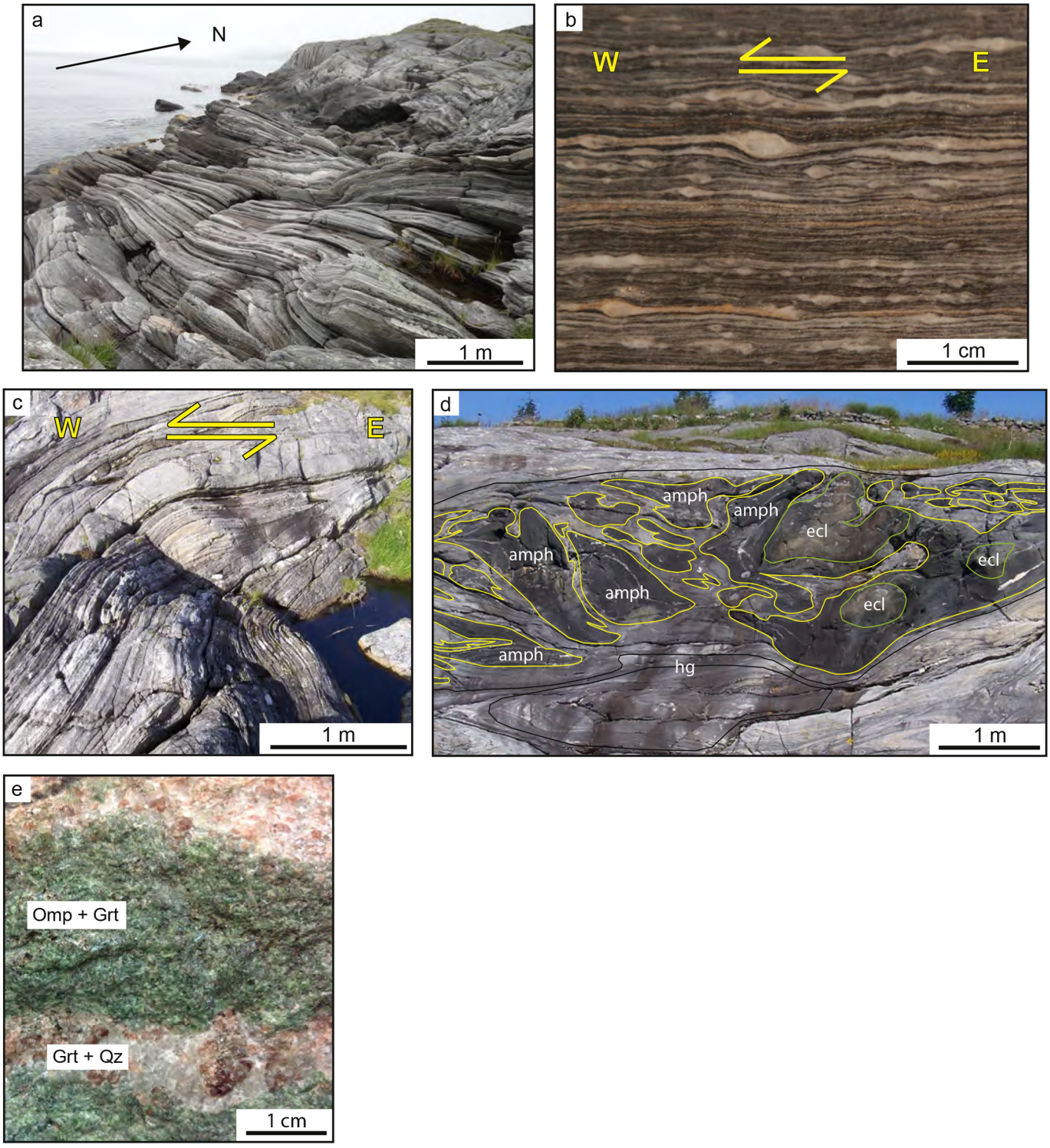

Fig. 3. Field photos of the SMZ. (a) Striped gneiss (e.g., sample NW10–40G) with consistent planar foliation and moderate N-dip. (b) K-feldspar porphyroclasts in striped gneiss showing top-to-the-west sense of shear. (c) Meter-scale fold in the striped gneiss of the SMZ that shows a westward vergence. (d) Retrogressed mafic pod at the northern end of the SMZ. Eclogite (ecl) cores what was likely an entire eclogite pod that has since retrogressed to amphibolite ± garnet (amph). It is surrounded by hornblende-bearing quartzofeldspathic gneiss (hg). The outlines delineate rock types but the contacts are gradational in nature. (d) Fresh, layered eclogite (e.g., samples NW10–40M, and NW11–21B and C) showing the relationship between foliation-parallel, quartz-rich layers and more abundant omphacite-rich layers. Mineral abbreviations after Whitney and Evans (2010).

δ morphologies (Passchier and Simpson, 1986) that indicate consistent top-to-the-west (left-lateral) sense of shear (Fig. 3b). A meter-scale fold that appears to have initiated around a large mafic pod also displays a westward vergence (Fig. 3c).

Metamorphosed mafic rocks (eclogite and amphibolite ± garnet) comprise ~10% of the SMZ and occur as layers and pods within the striped gneiss. Some amphibolite layers are thin (mm-to cm-scale) and show no clear relationship to eclogite; other amphibolites form the retrogressed rims of eclogite pods (Fig. 3d). The orientation of foliation in eclogite and amphibolite in the SMZ is consistent with the fabric in the host, striped quartzofeldspathic gneiss. However, the eclogite and amphibolite lineations display more variation than the gneiss lineation (Fig. 2b).

4. Mineral compositions and textures of eclogite and gneiss

Major element compositions of clinopyroxene in eclogite and plagioclase in gneiss were determined by electron-microprobe analysis (JEOL JXA-8900, Department of Earth Sciences, University of Minnesota Twin Cities). Qualitative (energy-dispersive spectroscopy) element maps were acquired using a 15 kV accelerating voltage, 100 nA current, a focused beam, and stage-rastering step sizes ranging from 1 to 3 μm depending on grain size. Quantitative (wavelength-dispersive spectroscopy) clinopyroxene analyses (to determine jadeite content) were acquired using a 15 kV accelerating voltage, 25 nA current, and a focused beam. Quantitative plagioclase analyses were acquired using a 15 kV accelerating voltage, 20 nA current, and a 5 μm beam. ZAF correction was applied to all analyses. Natural mineral standards were used for calibration. Representative compositions are in Table 1.

4.1. Eclogite

The primary, and best-preserved, occurrence of eclogite in the SMZ is a large, tabular eclogite outcrop that is 3–5 m thick and approximately 20 m long (samples NW10–40M, NW11–21B, C; Fig. 2a). This eclogite body contains a well-developed, shallowly to moderately N–NE dipping foliation and a subhorizontal E–W lineation. The foliation is defined by compositional layering between omphacite-rich layers and less abundant quartz-rich layers (mm-to cm-scale in thickness) (Figs. 3e and 4a). Elongate omphacite grains define the lineation. The edges of the eclogite body are retrogressed to amphibolite ± garnet. In the omphacite-rich layers the primary assemblage is omphacitic clinopyroxene (70–80 modal %; X_{Jd} = 0.34–0.57) + garnet (10–20%) + quartz (<10%) + rutile (<5%) with accessory zircon. The quartz-rich layers are composed of quartz (>65 modal %) + garnet (30%) + rutile (<5%) with accessory zircon.

Omphacite is coarse-grained (up to 6 mm long), elongate with an average aspect ratio of 3:1 (lineation–parallel plane), and typically does not display major-element zoning. Omphacite grain boundaries are ubiquitously replaced by symplectitic intergrowths of clinopyroxene + plagioclase or hornblende + plagioclase (Fig. 4b). Garnet is anhedral to subhedral in the omphacite-rich layers and subhedral in the quartz-rich layers. Garnet grains range in size from 0.5 to 6 mm and are typically larger in quartz-rich layers (>1 mm) than in omphacite-rich layers (<1 mm).

Quartz in eclogite occurs in three distinct habits: (1) as interstitial grains in the omphacite-rich regions, (2) in quartz-rich layers (Fig. 4a), and (3) as inclusions in garnet in quartz-rich layers (Fig. 4b). Quartz in omphacite-rich layers occurs as isolated grains or in clusters of up to four grains. The interstitial quartz is medium-grained (up to 1.5 mm), anhedral, and displays weak undulatory extinction. Quartz grains in quartz-rich layers are large (up to 3 mm diameter), irregular in shape, display strong undulatory extinction and highly sutured grain boundaries (Fig. 4c). Subgrains and recrystallized grains suggest recrystallization dominated by grain boundary migration (GBM) mechanisms (Hirth and Tullis, 1992; Stipp et al., 2002). Quartz-rich layers contain abundant garnets with quartz and Pcq inclusions. Quartz inclusions in garnet are typically single grains that show weak to no undulatory extinction. Pcq inclusions are observed only in garnets in quartz-rich layers, these inclusions range in size from 100 to 200 μm and are composed of numerous elongate quartz grains that radiate from the center of the inclusion (Fig. 4d).

4.2. Quartzofeldspathic gneiss

Quartzofeldspathic gneiss is the dominant rock type in the SMZ, as it is in the rest of the WGR. The striped gneiss within the SMZ (e.g., sample NW10–40G) and the coarser-grained, country-rock gneiss

Table 1
Representative mineral compositions of omphacite in eclogite and plagioclase in quartzofeldspathic gneiss.

Sample location lithology	Clinopyroxene				Sample location lithology	Plagioclase							
	NW11–31A in SMZ ecl		NW11–21B in SMZ ecl			NW10–40A out of SMZ Gn, Pl core		NW10–40A out of SMZ Gn, Pl rim		NW10–40G in SMZ Gn, Pl core		NW10–40G in SMZ Gn, Pl rim	
SiO_2	55.62		55.28		SiO_2	61.81		60.24		60.89		59.59	
TiO_2	0.07		0.07		Al_2O_3	24.47		25.62		25.41		26.21	
Al_2O_3	14.62		10.08		FeO	0.04		0.16		0.13		0.16	
FeO	3.55		2.59		CaO	5.24		6.64		6.20		7.35	
MnO	0.02		0.05		Na_2O	9.07		7.79		7.98		7.35	
MgO	7.30		10.89		K_2O	0.30		0.23		0.33		0.27	
CaO	11.43		15.40		Total	100.93		100.68		100.94		100.90	
Na_2O	7.69		5.34										
Total	100.31		99.91										
Si	1.95	2.00	1.96	2.00	Si	2.74	3.00	2.68	3.00	2.69	3.00	2.64	3.00
Al^{IV}	0.05		0.04		Al^{IV}	0.26		0.32		0.31		0.36	
Al^{VI}	0.56	1.03	0.39	1.04	Al^{VI}	1.00		1.00		1.01		1.01	
Ti	0.00		0.00		Fe	0.00		0.01		0.01		0.01	
Mg	0.38		0.57		Ca	0.24	1.00	0.31	1.00	0.29	1.00	0.35	1.00
Fe^{2+}	0.10		0.08		Na	0.77		0.68		0.68		0.63	
Mn	0.00		0.00		K	0.01		0.01		0.02		0.02	
Ca	0.43	0.98	0.59	0.97									
Na	0.52		0.38		Ab	76		68		69		63	
					An	23		31		29		35	
Jd	0.53		0.37		Or	1		1		2		2	

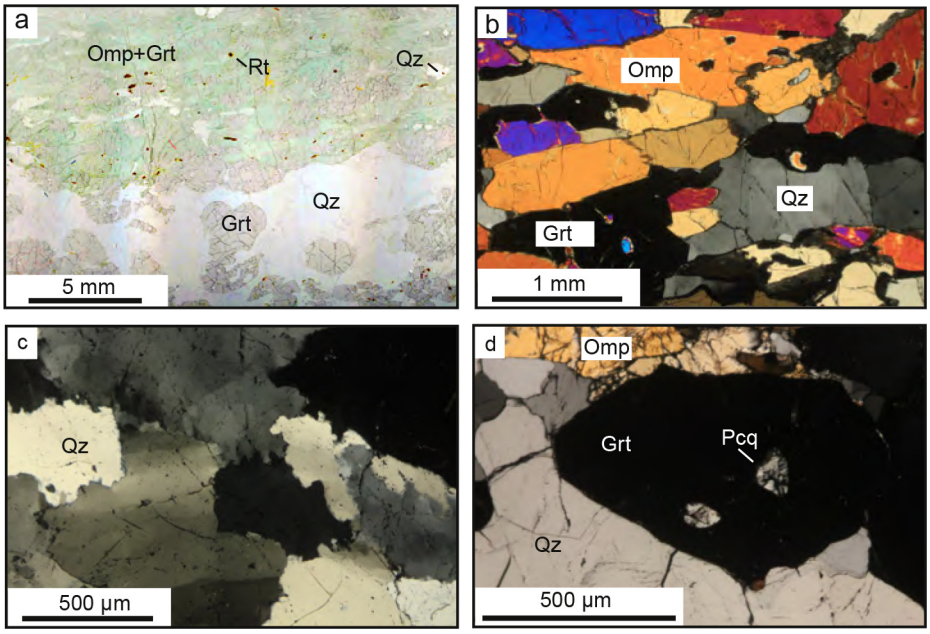

Fig. 4. Eclogite photomicrographs. (a) Thin section scan of coesite–eclogite (sample NW11–40M, lineation–parallel) showing a garnet-rich quartz layer within omphacite-rich regions. Garnets in the quartz-rich layer are larger and more euhedral than those in the omphacite-rich regions. (b) Omphacite-rich region of coesite–eclogite (sample NW11–21B, lineation–parallel) showing elongate habit of omphacite crystals. (c) Quartz in quartz-rich layer (sample NW10–40M, lineation–parallel) showing irregular grain boundaries and strong undulatory extinction. (d) Garnet porphyroblast in a quartz-rich layer (sample NW10–40M, lineation–parallel) that contains two polycrystalline quartz inclusions that show characteristic palisade texture.

outside of the SMZ (e.g., sample NW10–40A) have similar mineral assemblages and modal abundances. The gneiss is comprised of plagioclase (40–65 modal %) + quartz (15–40%) + biotite (>10%) ± hornblende ± epidote/allanite ± garnet with accessory oscillatory-zoned zircon, titanite, magnetite and rare ilmenite and apatite. Though both gneiss types preserve the same assemblage, they display fabric and textural differences.

In the striped gneiss, quartz occurs in monomineralic, foliation-parallel ribbons that contain high aspect ratio quartz grains (~100 × 350 μm) (Fig. 5a). The ribbons are one grain thick, and quartz grain boundaries are straight and perpendicular to the ribbon boundaries. Some quartz grains show undulatory extinction. Quartz ribbons are longer in lineation–parallel planes (>5 cm) than in lineation–perpendicular planes (<1 cm).

The regions between quartz ribbons are dominated by plagioclase but also contain biotite, epidote, titanite, and hornblende in varying amounts, and rare, highly disaggregated garnet. Plagioclase in the striped gneiss occurs as small, equant grains (~100 μm diameter) with straight edges, triple junctions with 120° interfacial angles, and rare twins (granoblastic texture). Plagioclase displays optically visible zoning (Fig. 5b). Electron-microprobe analysis reveals that the plagioclase is reverse zoned (Fig. 5c). Plagioclase preserves more sodic cores (~An_{30}) and more calcic rims (~An_{40}); the average ΔAn from core to rim is 10 mol%. Zoning is observed in nearly all grains in the striped gneiss. Some small grains do not display zoning, most likely because of a sectioning effect (the center of the grain is not on the plane of the thin section) or a size effect (the grain is sufficiently small such that during recrystallization the whole grain was replaced with a new, more calcic grain). Potassium feldspar porphyroclasts are partially to fully replaced by subgrains (~150 μm diameter) that lack internal distortion (Fig. 5d).

Differences between the striped gneiss of the SMZ and the country-rock gneiss are primarily related to grain size and grain-boundary geometry. Quartz occurs in foliation-parallel ribbons in both gneiss types, but in the country-rock gneiss the grain size is larger (0.5 × 1.5 mm), grains more commonly display undulatory extinction, and grain boundaries are curved (Fig. 5e). Plagioclase grains in the country-rock gneiss are coarser (typically 250–300 μm diameter), display more abundant twinning, and exhibit serrated grain boundaries. Plagioclase grains in the country-rock gneiss also display core-to-rim reverse zoning (Fig. 5f), but the compositional variation from core (~An_{25}) to rim (~An_{31}) is less distinct than in the striped gneiss with an average ΔAn from core to rim of 6 mol%. Biotite crystals (~250 μm × 1 mm long) are aligned parallel to the principal foliation and occur as isolated grains. Potassium feldspar porphyroclasts are largely made of equant, strain-free subgrains and new grains (~250 μm diameter).

5. Ti-in-quartz thermobarometry

Ti-in-quartz thermobarometry was applied to eclogite and gneiss from the SMZ. This trace-element thermobarometer is used to build on previous major-element thermobarometry (Wain, 1997) to reconstruct *P*–*T* conditions for eclogite and gneiss in the SMZ. Ti-in-quartz thermobarometry is based on the *P*- and *T*-dependent substitution of Ti into silica tetrahedra in the quartz structure; Ti solubility increases as *P* decreases and as *T* increases. Two widely-used calibrations of this thermobarometer have been proposed, first by Wark and Watson (2006) and Thomas et al. (2010) (includes a dependence on a_{TiO2}), and second by Huang and Audétat (2012) (independent of a_{TiO2}). Over the range of pressures of interest for this study (1.0 GPa < *P* < 2.8 GPa), the Thomas et al. (2010) calibration is significantly more pressure sensitive than the Huang and Audétat (2012) calibration. The calibrations cross over at 2 GPa. As it is unclear which calibration is more appropriate for this study we report results using both.

Titanium concentration ([Ti]) in quartz was measured using secondary ion mass spectrometry (SIMS) at the Northeast National Ion Microprobe Facility (NENIMF) at Woods Hole Oceanographic

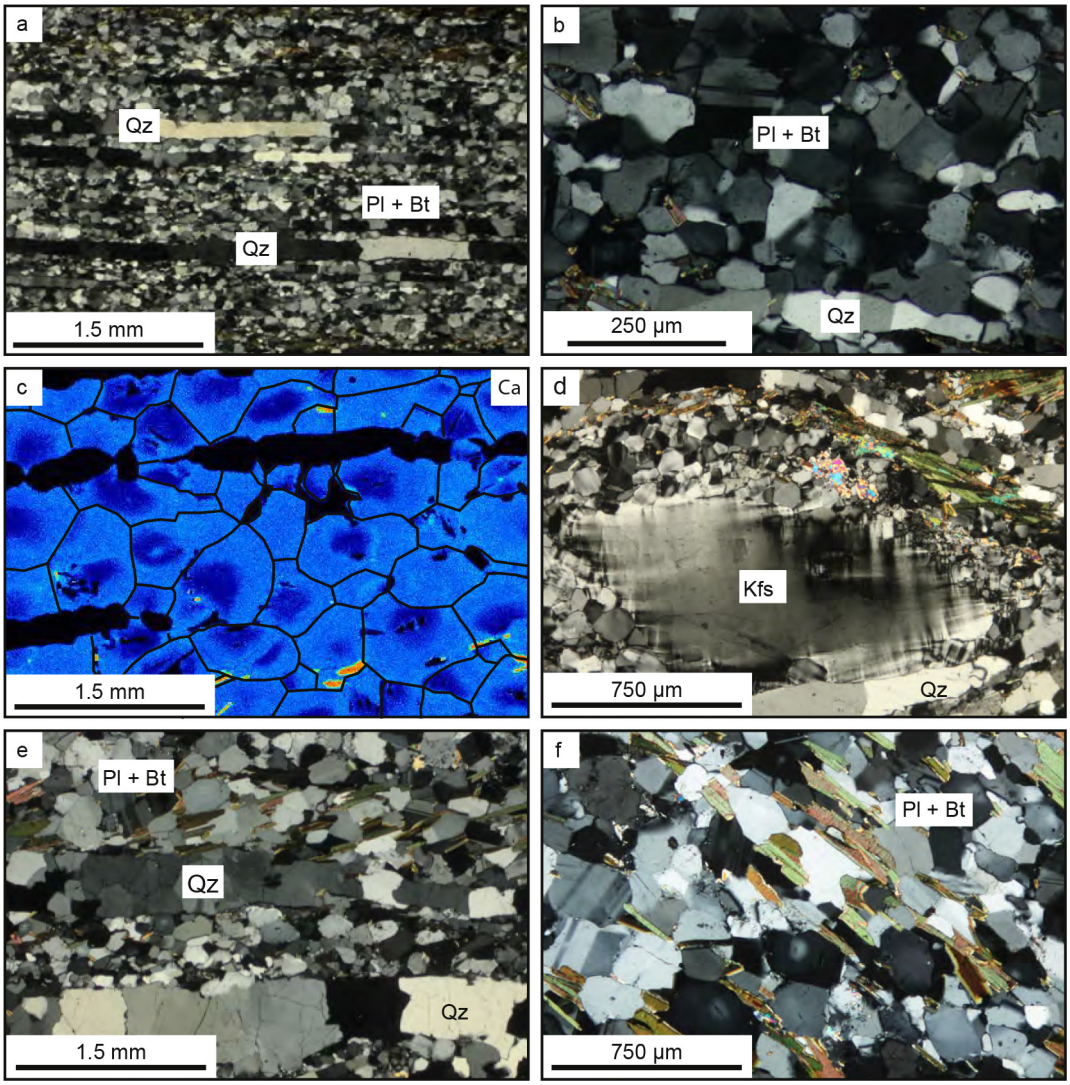

Fig. 5. Quartzofeldspathic gneiss photomicrographs within and outside of the SMZ. (a) Striped gneiss (sample NW10–40G, lineation–parallel) showing characteristic foliation-parallel quartz ribbons. Recrystallized plagioclase and biotite comprise the regions between quartz ribbons. (b) Recrystallized plagioclase in striped gneiss (sample NW10–40G, lineation–parallel). The plagioclase displays optically visible reverse zoning, lacks twinning, and commonly displays straight grain boundaries and triple junctions. (c) Ca element map of plagioclase in striped gneiss (sample NW10–40G, lineation–parallel). This element map shows the reverse compositional zoning preserved in plagioclase with lower An cores and higher An rims. Grain boundaries were superimposed on the image. (d) Partially recrystallized K-feldspar porphyroclast in striped gneiss (sample NW10–40F, lineation–parallel). Quartz ribbons wrap the asymmetric porphyroclast. (e) Country-rock gneiss (sample NW10–40A, lineation–parallel) showing characteristic foliation-parallel quartz ribbons. Quartz–quartz grain boundaries are serrated and grains commonly display undulatory extinction. Plagioclase and biotite comprise the regions between quartz ribbons. Grain size in the country-rock gneiss is significantly larger than in the striped gneiss. (f) Country-rock gneiss (sample NW10–40A, lineation–parallel) showing optically visible reverse zoning in plagioclase. The plagioclase displays frequent twinning and serrated grain boundaries.

Institution following the analytical process of Nachlas et al. (2014). Analytical error for SIMS [Ti] measurements reported in this study is ±0.1 ppm; this error corresponds to <1 °C difference in *T* estimate after either calibration. The effect of the analytical error is significantly smaller than the error associated with the thermodynamic parameters used to derive the calibrations; therefore error is not provided in the thermobarometry results. Four data points were omitted due to contamination with excess calcium indicating intersection with a secondary phase or grain boundary. Qualitative trace-element variation in quartz was assessed using cathodoluminescence (CL). This was completed using a JEOL 6500 FEG–SEM (Characterization Facility, University of Minnesota Twin Cities) equipped with a Gatan MonoCL 2 System. Previous studies (e.g. Müller et al., 2003) have documented a correlation between CL and Ti content, here we use CL as a qualitative proxy for Ti content in quartz.

In rutile-bearing eclogite from the SMZ (sample NW11–21B), [Ti] was analyzed in quartz in quartz-rich layers (Fig. 4c) and in quartz inclusions in garnet (Fig. 4d). Quartz in these textural locations preserves similar [Ti]: 5.2–6.9 ppm ($n = 16$), with a mean [Ti] of 6.2 ± 0.6 ppm (Fig. 6, Table 2). The small range in [Ti] in eclogite allows us to use the mean [Ti] for the thermobarometry (Fig. 7). CL images of quartz in eclogite suggest that quartz grains in both settings are largely homogeneous with respect to Ti content, but reveal the presence of numerous darker, healed fractures or veins that are not observable with visible light spectroscopy.

The minimum peak *P* for this eclogite body is 2.8 GPa (Wain, 1997). If this corresponds to the *P* at which [Ti] equilibrated in the quartz, then the calculated temperature ($a_{TiO2} = 1$, rutile present) is 831 °C after Thomas et al. (2010) and 739 °C after Huang and Audétat (2012) (Fig. 7, Table 3). If [Ti] equilibrated at $P = 2.0$ GPa (quartz stable, eclogite-facies conditions), then the

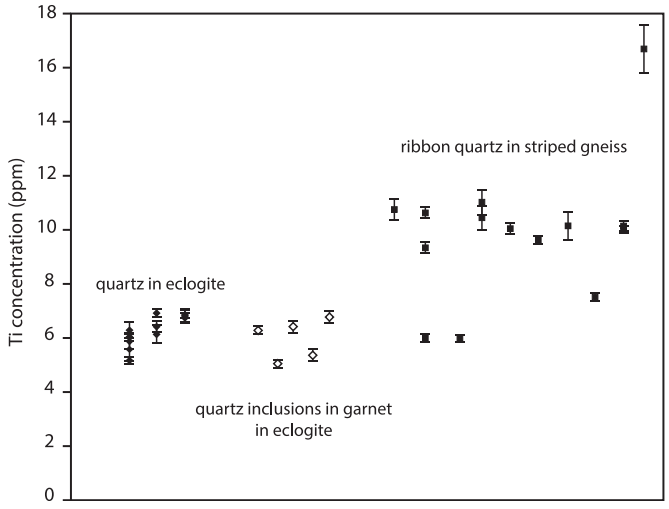

Fig. 6. Graph of [Ti] in quartz by lithology and habit. Quartz in eclogite, both in the quartz-rich layers and as inclusions in garnet, preserves similar [Ti]. [Ti] in quartz in quartzofeldspathic gneiss displays considerable variation within grains (each column of data corresponds to one grain) and among grains. Error bars are 1 standard deviation.

calculated temperature using both calibrations coincide at 690 °C ($a_{TiO2} = 1$, rutile present). Results of Ti-in-quartz thermobarometry for this eclogite broadly agree with previous major-element thermobarometry results for UHP eclogite in this region (~740–840 °C, Wain, 1997).

Table 2
Ti concentration (measured by SIMS) in quartz in eclogite and quartzofeldspathic gneiss. Gray shading identifies data points that were omitted due to contamination.

	Point	[Ti] (ppm)		Site
		Mean	Standard deviation	
Quartzofeldspathic gneiss (NW10–40G)	50	10.8	0.4	Qz ribbon
	51	10.7	0.2	Qz ribbon
	52	9.4	0.2	Qz ribbon
	53	6.0	0.2	Qz ribbon
	54	6.0	0.1	Qz ribbon
	55	11.0	0.5	Qz ribbon
	56	10.5	0.4	Qz ribbon
	57	2.0	−0.1	Qz ribbon
	58	2.0	0.2	Qz ribbon
	59	10.1	0.2	Qz ribbon
	60	9.6	0.2	Qz ribbon
	61	10.2	0.5	Qz ribbon
	62	7.5	0.1	Qz ribbon
	63	10.0	0.1	Qz ribbon
	64	10.2	0.2	Qz ribbon
	65	16.7	0.9	Qz ribbon
Eclogite (NW11–21B)	86	5.2	0.2	Qz layer
	87	5.9	0.3	Qz layer
	88	6.3	0.3	Qz layer
	89	5.6	0.4	Qz layer
	90	6.1	0.1	Qz layer
	91	6.1	0.3	Qz layer
	92	6.4	0.2	Qz layer
	93	6.9	0.2	Qz layer
	94	6.8	0.2	Qz layer
	95	6.9	0.1	Qz layer
	96	6.8	0.2	Qz layer
	97	6.9	0.1	Inclusion
	98	70.6	2.6	Inclusion
	99	5.1	0.1	Inclusion
	100	91.0	7.3	Inclusion
	101	6.4	0.2	Inclusion
	102	5.4	0.2	Inclusion
	103	6.8	0.2	Inclusion

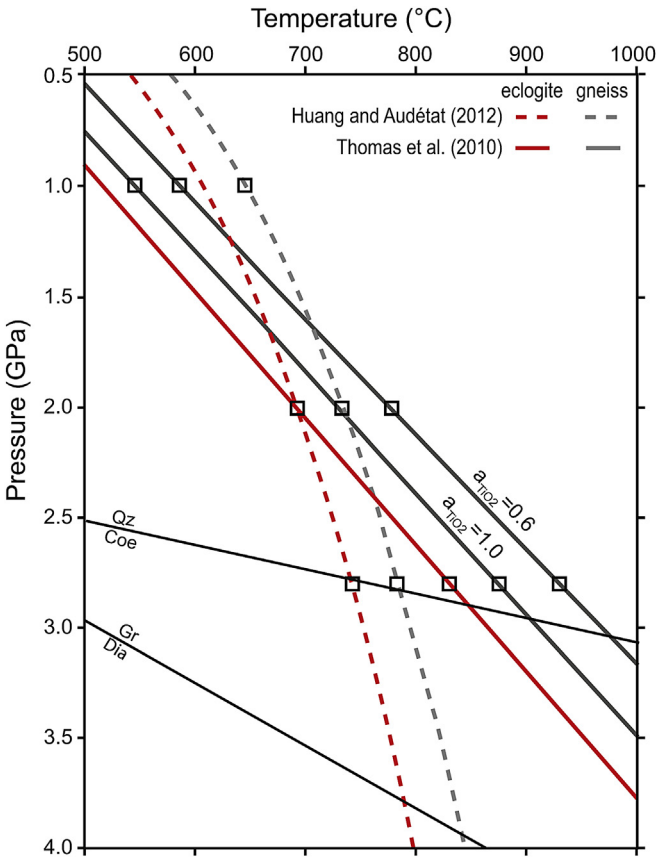

Fig. 7. *P–T* diagram summarizing results of eclogite and gneiss Ti-in-quartz thermobarometry. This graph shows *P–T* curves of the two calibrations for both lithologies over the *P* and *T* range of interest for this study plotted using the mean [Ti] for each lithology (6.2 ppm for eclogite and 9.9 ppm for gneiss). The Thomas et al. (2010) calibration includes two calculations for gneiss (solid gray lines) due to the presence of titanite, one using $a_{TiO2} = 0.6$ and one using $a_{TiO2} = 1.0$, and one calculation for eclogite ($a_{TiO2} = 1$, solid red line). Calculations resulting from Huang and Audétat (2012) are shown in dashed lines (gneiss – gray, eclogite – red). Pressures of interest ($P = 2.8$, 2.0, and 1.0 GPa, see text) are highlighted on each calibration by a small box in order to show the range of temperature estimates for each scenario. (For interpretation of the references to color in this figure legend, the reader is referred to the web version of this article.)

In the striped gneiss, [Ti] in quartz was measured in multiple ($n = 5$) quartz ribbons, and as transects within individual grains (up to 3 points per grain). [Ti] in quartz varies from 6.0 to 16.7 ppm ($n = 14$), with a mean [Ti] of 9.9 ± 2.6 ppm. The maximum observed intergranular variation in [Ti] is 10.7 ppm, and the maximum intragranular variation is 4.6 ppm (Fig. 6, Table 2). CL images reveal two main patterns: (1) quartz grains with a bright core and a darker rim and (2) quartz grains with a mottled pattern. These variations do not directly correspond with differences in measured [Ti].

Application of Ti-in-quartz thermobarometry to the striped gneiss is complicated due to the absence of rutile and presence of titanite in the system, which introduces uncertainty in a_{TiO2}. For titanite-bearing systems, a_{TiO2} can range from 0.6 to 1.0 (Ghent and Stout, 1984; Behr and Platt, 2011). Therefore, *T* estimates using the Thomas et al. (2010) calibration were calculated with $a_{TiO2} = 0.6$ and 1.0, then compared to assess the spread in *T* estimate as a function of changing a_{TiO2}. Huang and Audétat (2012) assume $a_{TiO2} = 1$ and do not allow for a_{TiO2} variation; therefore, *T* estimates at a given *P* are considered a minimum. For this range of [Ti], *T* estimates resulting from an input of $a_{TiO2} = 0.6$ yield estimates up to 50 °C lower than those calculated with $a_{TiO2} = 1$ at a given *P*. Since *P* at the time of equilibration of Ti in quartz within the gneiss

Table 3
Temperature estimates resulting from Ti-in-quartz thermobarometry.

Calibration	Pressure (GPa)	a_{TiO2}	Quartzofeldspathic gneiss			Eclogite
			Minimum [Ti] (5.99 ppm)	Mean [Ti] (9.90 ppm)	Maximum [Ti] (16.73 ppm)	Mean [Ti] (6.30 ppm)
Thomas et al. (2010)	2.8	1	828 °C	876 °C	931 °C	831 °C
		0.6	877 °C	930 °C	990 °C	n/a
	2.0	1	688 °C	730 °C	778 °C	691 °C
		0.6	731 °C	777 °C	830 °C	n/a
	1.0	1	514 °C	548 °C	587 °C	n/a
		0.6	549 °C	586 °C	629 °C	n/a
Huang and Audétat (2012)	2.8		736 °C	784 °C	838 °C	739 °C
	2.0		688 °C	733 °C	785 °C	691 °C
	1.0		605 °C	646 °C	693 °C	n/a

is uncertain, we calculated temperatures for three scenarios that represent the possible range of P of Ti equilibration in quartz: (1) P in the gneiss was at UHP conditions, the same as recorded by the eclogite (>2.8 GPa); (2) P in the gneiss was high, but lower than recorded by the eclogite (2.0 GPa) and (3) P was substantially lower than that of the eclogite and consistent with amphibolite-facies equilibration (1.0 GPa). Because [Ti] in quartz is variable, with no systematic zoning, we considered the minimum, average, and maximum values of [Ti] for each scenario.

Temperature estimates for the striped gneiss (Fig. 7, Table 3) range from 514 °C to 990 °C depending on input parameters. Temperature estimates based on maximum [Ti] are 75–115 °C higher than those based on minimum [Ti] (Table 3). Temperature estimates based on mean [Ti] fall in between those estimates based on maximum and minimum [Ti] (presented herein and displayed in Fig. 7). At $P = 2.8$ GPa (scenario 1), T estimates are 876 °C ($a_{TiO2} = 1$) and 930 °C ($a_{TiO2} = 0.6$) using the calibration of Thomas et al. (2010) and 784 °C using the calibration of Huang and Audétat (2012). At $P = 2.0$ GPa (scenario 2), T estimates using the calibration of Thomas et al. (2010) and Huang and Audétat (2012) coincide at 730 °C ($a_{TiO2} = 1$), with a higher T estimate of 777 °C corresponding to $a_{TiO2} = 0.6$ using the calibration of Thomas et al. (2010). At $P = 1.0$ GPa (scenario 3), T estimates are 548 °C ($a_{TiO2} = 1$) and 586 °C ($a_{TiO2} = 0.6$) using the calibration of Thomas et al. (2010) and 646 °C using the calibration of Huang and Audétat (2012).

Additional uncertainties related to our application of this thermobarometer are: the rocks most likely equilibrated at much higher pressures ($P > 2$ GPa for the eclogite) than the calibration conditions, and it is not known how the transformation of coesite to quartz (and vice versa) affects the solubility of Ti in quartz (Thomas et al., 2012). Despite uncertainty in the details of the Ti-in-quartz thermobarometry there is a significant difference in the [Ti] between eclogite and gneiss. The difference in [Ti] reflects the conditions of Ti equilibration conditions, higher T for the eclogite (near the quartz–coesite transition), and lower T for the gneiss (amphibolite-facies).

6. Microstructural analysis: EBSD

The crystallographic orientation of minerals in gneiss and eclogite in the SMZ is used to evaluate grain-scale deformation mechanisms during ductile shear zone evolution. Crystallographic

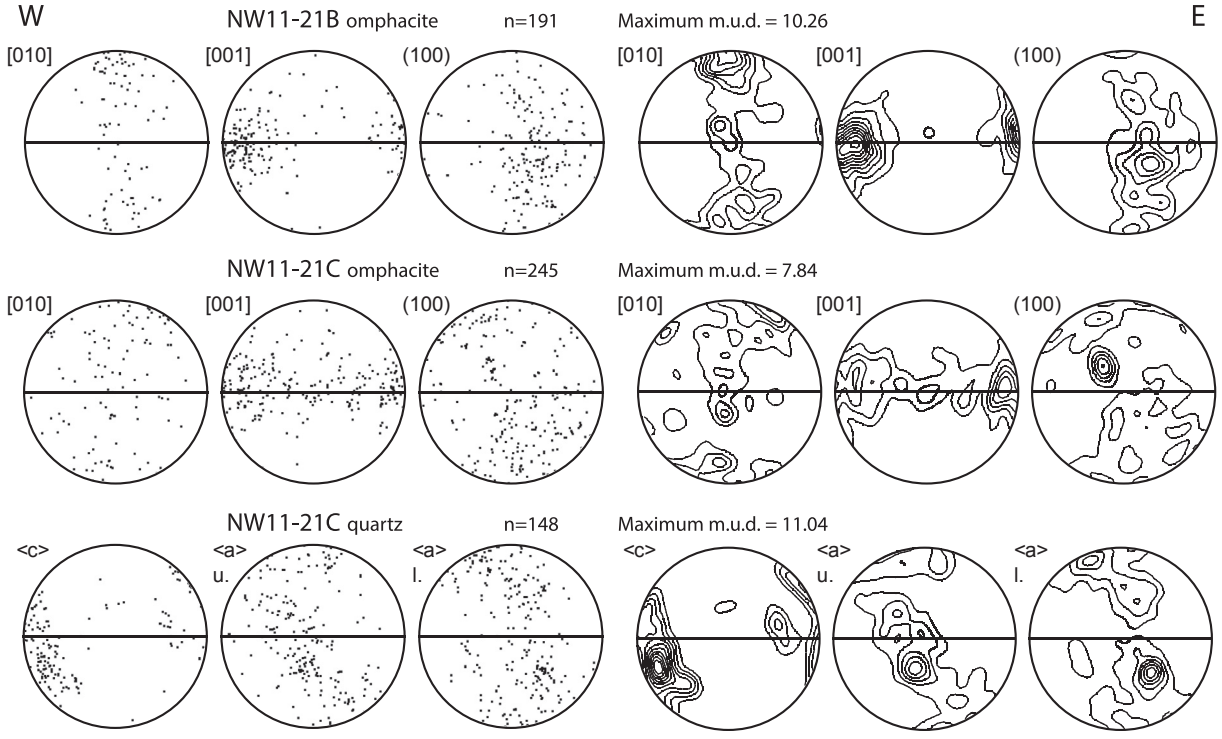

Fig. 8. Omphacite and quartz fabrics from eclogite (samples NW11–21B and C). Data is displayed as point data on the left and as contoured plots (contoured in multiples of 1 m.u.d.) on the right. Upper (u.) and lower (l.) hemisphere data plotted for quartz.

fabrics were measured by electron backscatter diffraction (EBSD) analysis. Thin-section preparation included polishing with diamond paste to 1 μm grit size followed by SYTON polishing (1.5–2 h) in order to maximize indexing. Samples were coated with a thin carbon coat prior to analysis. EBSD data for omphacite and quartz in eclogite were acquired at the University of Minnesota–Duluth's Research Instrumentation Laboratory with a JEOL 6500 FEG scanning electron microscope (SEM) equipped with an Oxford Instruments NordlysS detector and HKL Channel 5 software. SEM conditions were 20 kV accelerating voltage, 4 nA beam current, working distance of 23 mm, and dynamic focus for 70° sample tilt. These data were collected as a series of maps with a 50 or 100 μm step size and covered areas approximately 1 × 2 cm. EBSD data for quartz in gneiss were acquired at Macquarie University with a Zeiss EVO SEM equipped with an Oxford Instruments NordlysMax detector and the Aztec Software package. SEM conditions were 20 kV accelerating voltage, 8 nA beam current, working distance of 12–14 mm, and dynamic focus for 70° sample tilt. Step sizes ranged from 3 to 6 μm and covered areas of approximately 3 × 3 mm.

EBSD data analysis was completed using HKL Channel 5 post-processing software. The reference coordinates (*XYZ*) were defined according to the macroscopic foliation and lineation: *X* is parallel to the lineation, *Y* is orthogonal to the lineation, and *Z* is perpendicular to the foliation. All data are plotted as one point per grain on lower hemisphere, equal area projections. In the case of quartz we also present upper hemisphere projections. Pole figures are shown as both point plots and contoured plots (contoured at multiples of 1 multiple of uniform distribution, m.u.d.). The number of grains (*n*) and the maximum m.u.d. are given for each sample.

6.1. Eclogite fabrics

Two eclogite samples from the fresh, layered eclogite body in the SMZ were selected for EBSD analysis. Sample NW11–21B consists of omphacite-rich eclogite with garnet and interstitial quartz. Sample NW11–21C includes omphacite-rich eclogite as well as a garnet-bearing quartz layer.

Omphacite in NW11–21B (Fig. 8, top) shows a strong crystallographic preferred orientation (CPO) with [001]-axes forming a point maximum parallel to the lineation and [010]-axes forming a point maximum normal to the lineation. The (100)-poles are less organized but form a weak girdle sub-perpendicular to the lineation. Omphacite in NW11–21C (Fig. 8, middle) shows a similar pattern; the [001]-axes form a girdle in the plane of the foliation with the largest concentration of axes nearly lineation–parallel, and the [010]-axes and (100)-poles both form weak, partial girdles at a high angle to the lineation. The macroscopic mineral fabric of omphacite is consistent with the observed crystallographic fabrics (the long axis of omphacite grains is parallel to the *c*-axis).

Though quartz occurs in multiple habits in the eclogite, we measured the crystallographic fabrics of quartz from the quartz-rich layers because it shows clear evidence of dynamic recrystallization during fabric development (Fig. 4c). Quartz preserves a strong CPO with the *c*-axes forming a point maximum oblique (~20°) to the lineation and *a*-axes forming a partial, inclined girdle nearly normal to the *c*-axis concentration (Fig. 8, bottom).

6.2. Quartzofeldspathic gneiss fabrics

Quartz fabrics from ribbons in quartzofeldspathic gneiss were analyzed in two samples from the Salt region, one country-rock gneiss from outside of the SMZ (sample NW10–40A) and one striped gneiss within the SMZ (sample NW10–40G). Quartz from the gneiss outside of the SMZ displays a fabric of moderate strength. The *c*-axes form a girdle perpendicular to lineation, and the *a*-axes are fairly evenly distributed on the primitive circle (Fig. 9, top). Quartz from the gneiss within the SMZ shows a similar, though stronger, CPO with a partial girdle of *c*-axes perpendicular to the lineation and *a*-axes distributed around the primitive circle with point maxima concentrations (Fig. 9, bottom). The striped gneiss shows a stronger concentration of *a*-axes on the great circle than the country-rock gneiss.

7. Discussion

7.1. Fabric development from high-to medium-pressure conditions

Omphacite in UHP eclogite in the SMZ is elongate and defines the foliation. One sample (NW11–21B) shows an omphacite fabric (Fig. 8) with a point maximum of [001]-axes parallel to the lineation and a diffuse girdle of [010]-axes normal to the lineation. A second eclogite sample (NW11–21C) has a weak girdle of [001]-

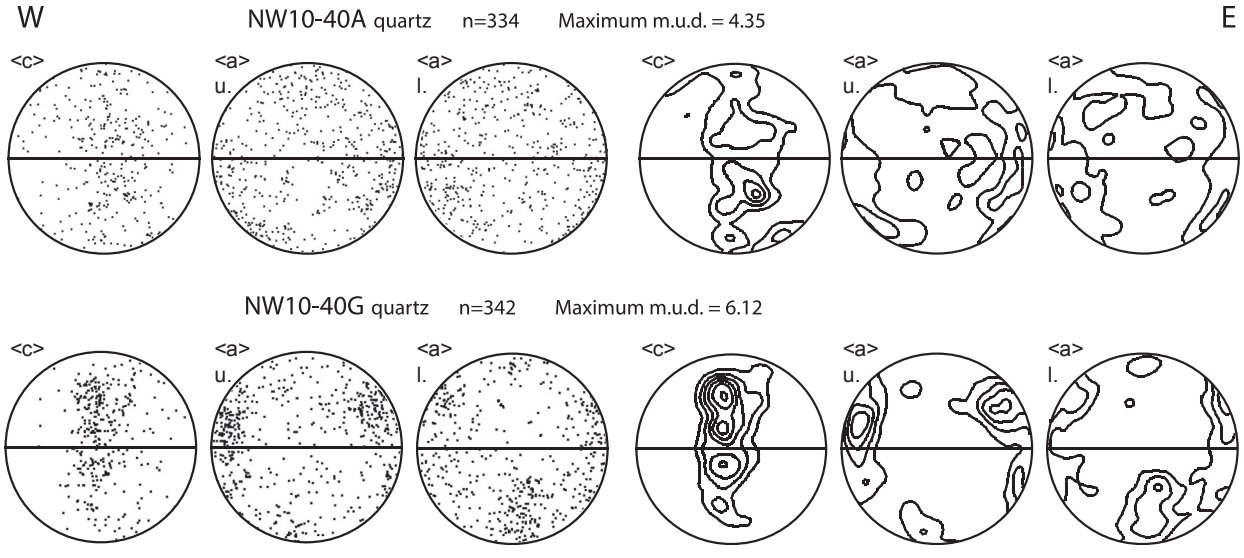

Fig. 9. Quartz fabrics from striped (top, sample NW10–40G) and country-rock (bottom, sample NW10–40A) gneiss. Data is displayed as point data on the left and as contoured plots (contoured in multiples of 1 m.u.d.) on the right. Upper (u.) and lower (l.) hemispheres displayed.

axes in the plane of the foliation and an asymmetric partial girdle of [010]-axes near-normal to the lineation. These fabrics are best characterized as L- to LS-type patterns and are thought to develop during constrictional deformation and plane strain (Helmstaedt et al., 1972; Boundy et al., 1992; Godard and van Roermund, 1995). L-type CPO have been generated experimentally in simple shear (Zhang et al., 2006; Zhang and Green, 2007), in models of pure shear and simple shear (Bascou et al., 2001), as well as in models of transtension (Bascou et al., 2002). Omphacite fabrics developed in models of transtension show a CPO with a girdle of [010]-axes perpendicular to lineation, as opposed to point maxima (Bascou et al., 2002). LS-type fabrics are intermediate fabrics between L- and S-type end-members, and this fabric pattern likely represents a combination of conditions that generate L- and S- type fabrics (Ábalos, 1997).

Similar omphacite fabrics to the ones presented in this study (L- and LS-type patterns) have been reported from other eclogites in the WGR from the Nordfjord UHP domain as well as in the Sulu UHP terrane of China (Bascou et al., 2001; Zhang and Green, 2007). Asymmetric omphacite fabrics have been documented in naturally-deformed eclogite samples (Ábalos, 1997; Mauler et al., 2000; Bascou et al., 2001) and have been interpreted as a consequence of non-coaxial deformation.

Quartz in the SMZ eclogite records a strong, asymmetric CPO generated by activation of the prism <c> slip system. Activation of this slip system is accomplished by high-*T* deformation, as well as likely water-present conditions (Tullis, 1977; Blumenfeld et al., 1986; Mainprice et al., 1986). The asymmetry in the *c*-axis orientation presented here is consistent with a sinistral sense of shear (Blumenfeld et al., 1986; Garbutt and Teyssier, 1991), which is consistent with kinematic indicators in the ductile deformation zone and, more broadly, with motion on the Møre-Trondelag fault zone.

Similar quartz fabrics to the one presented in this study have been recently documented in HP/UHP eclogites from the Sulu terrane (Zhang et al., 2013). This study also shows that coesite develops a weak fabric in naturally deformed eclogite. Though the SMZ eclogite reached UHP conditions, as evidenced by the presence of Pcq, the prism <c> fabric preserved in the quartz-rich layers developed during deformation under HP, quartz-stable conditions

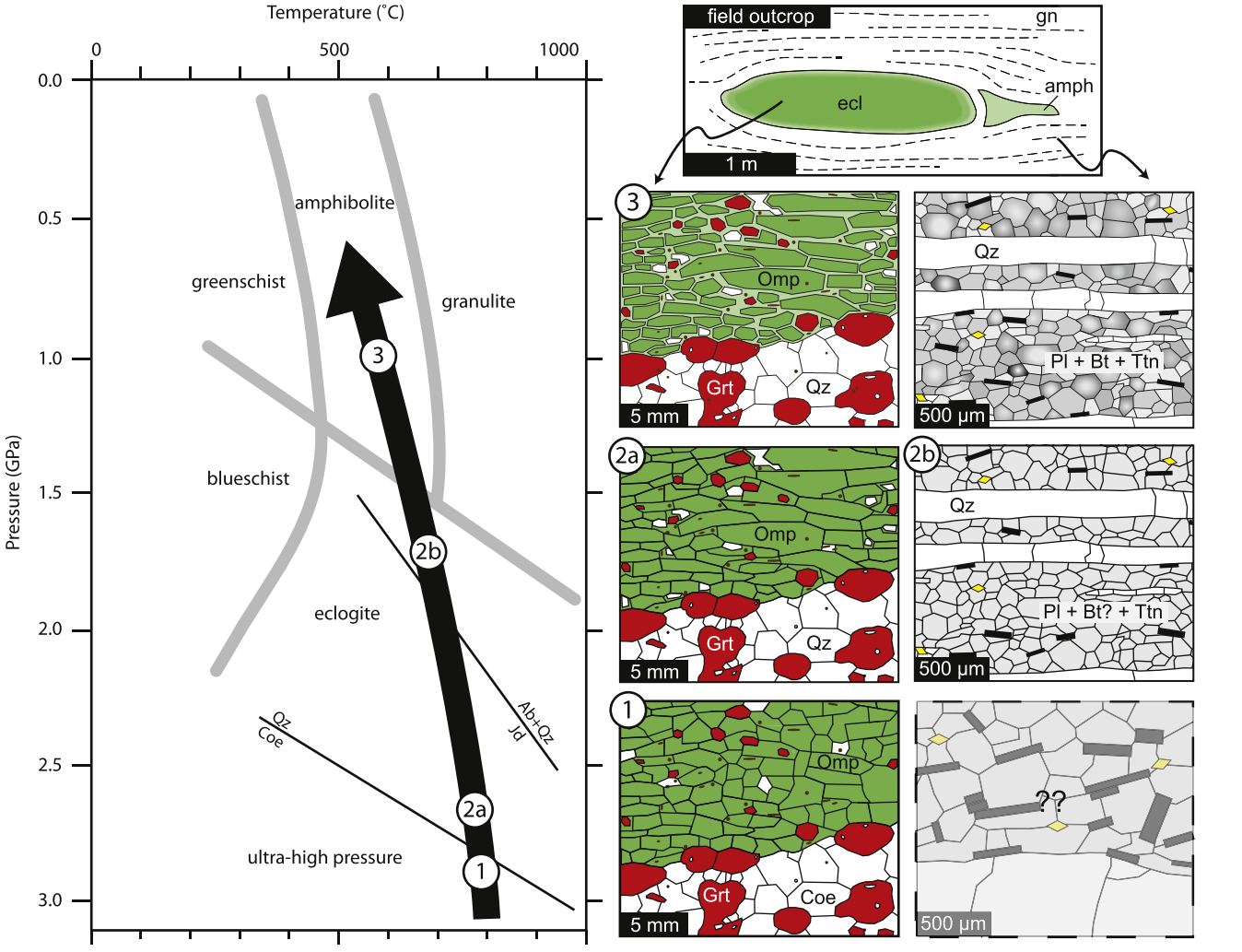

Fig. 10. Schematic figure showing the fabric development during exhumation and decompression of the SMZ. Phase 1: Eclogite (and likely gneiss, at least locally) experienced ultrahigh-pressure (coesite-stable) conditions prior to fabric development. Phase 2a: At HP conditions (quartz stable), omphacite and quartz fabrics in eclogite developed. The Ti-in-quartz thermobarometry suggests temperatures from 750 to 830 °C for this phase. Phase 2b: Quartz fabrics in quartzofeldspathic gneiss began to develop. Plagioclase is Na-rich (lighter gray). Phase 3: By amphibolite-facies (mid-crustal) conditions, the eclogite developed a Hbl + Pl symplectite that variably replaces Omp−Omp grain boundaries. Dynamic recrystallization of plagioclase at continually decreasing pressures led to the development of reverse zoning (represented by darker gray rims). Quartz in quartzofeldspathic gneiss may have continued to develop fabrics down to *P* of ~1 GPa where Ti-in-quartz thermobarometry *T* estimates range from ~515 to 700 °C.

near the quartz–coesite transition. The similarity of [Ti] in quartz inclusions in garnet with quartz in the quartz-rich layers supports that the quartz deformation in the eclogite occurred at high *T* and suggests that the quartz, and possibly omphacite as well, was not extensively altered by subsequent deformation and/or recrystallization (i.e., the quartz did not continue to deform or equilibrate as the rocks were exhumed).

Quartz in the striped and country-rock gneiss preserves fabrics generated by consistently lower *T* deformation than those in the eclogite. The country-rock gneiss displays a diffuse quartz CPO (Fig. 9, top) that includes evidence of activation of the basal, prism, and rhomb <a> slip. Quartz fabrics in the striped gneiss (Fig. 9, bottom) suggest that quartz deformed in the dislocation creep regime with activation of the prism <a> and rhomb <a> slip systems. The lack of evidence for basal <a> slip in the striped gneiss suggests that this fabric developed at higher *T* than the country-rock gneiss (Stipp et al., 2002). No significant asymmetry in CPO patterns of quartz in gneiss is observed.

7.2. Proposed model of ductile shear zone evolution

The SMZ comprises UHP eclogite and now amphibolite-facies quartzofeldspathic gneiss. The eclogite in the SMZ experienced UHP conditions (Fig. 10, phase 1) as indicated by Pcq inclusions (e.g., Fig. 4d) and rare coesite inclusions (e.g., Carswell et al., 2003a) in garnet. Concordance of foliation and lineation orientations in gneiss and eclogite and rare petrographic evidence (e.g. Pcq inclusions in gneiss, Wain, 1997) suggest that the quartzofeldspathic gneiss also experienced UHP conditions, at least locally. Therefore, despite the fact that the gneisses in this study do not preserve obvious evidence for UHP conditions, it is likely that the gneiss and associated mafic inclusions were deformed in a similar kinematic framework over a shared *P–T* path during exhumation from mantle depths.

During the initial stages of exhumation (Fig. 10, phase 2, passing into the quartz stability field) eclogite fabrics developed, including a quartz CPO generated by prism <c> slip and LS- to L-type omphacite CPO patterns. Ti-in-quartz thermobarometry in eclogite suggests high-*T* deformation (~750–830 °C). This *T* estimate is consistent with the dominant activation of the prism <c> slip system in quartz. The omphacite fabrics in this study are consistent with deformation during constriction and/or plane strain, with no evidence of flattening. Amphibolite-facies constrictional fabrics are well documented in the WGR and have been interpreted as indicative of transtension (Krabbendam and Dewey, 1998; Terry and Robinson, 2003; Barth et al., 2010). The omphacite fabrics reported in this study might also be interpreted as a result of transtension at HP to nearly UHP conditions.

It is not clear when strain localization occurred during the exhumation/decompression history and when the SMZ initiated. However, structures and fabrics consistent with deformation and metamorphism at amphibolite-facies conditions are now widespread (Fig. 10, phase 3). Amphibolite-facies retrogression in the eclogite is indicated by the presence of hornblende + plagioclase symplectite that variably replaces omphacite grain boundaries. Plagioclase reverse zoning (Figs. 5c and 10, phase 3) suggests plagioclase recrystallization and growth during continued decompression. *T* estimates from Ti-in-quartz thermobarometry at crustal depths ($P = 1.0$ GPa) range from 550 to 650 °C, consistent with the observed amphibolite-facies assemblages and fabrics.

In summary, the SMZ preserves a suite of fabrics in eclogite and quartzofeldspathic gneiss that record decompression from UHP conditions to mid-crustal levels. Eclogite contained within the gneiss preserves prism <c> quartz fabrics and LS- to L-type omphacite fabrics, and Ti-in-quartz thermobarometry suggests deformation at *P* and *T* conditions near the quartz–coesite transition. The host gneiss preserves quartz fabrics consistent with activation of the prism and rhomb <a> slip systems in quartz and reverse zoning in plagioclase owing to continued recrystallization during decompression to amphibolite-facies conditions (<650 °C based on to Ti-in-quartz thermobarometry).

Acknowledgments

We would like to acknowledge funding from NSF grants EAR-1040980 and EAR-0911497 to Whitney and Teyssier. We thank Dr. Brian Bandli for EBSD analyses of eclogite and Dr. Nicholas Seaton for help with EBSD data analysis. SP acknowledges funding by the Australian Research Council (DP120102060, FT110100070). We also thank Benito Ábalos, Florian Heidelbach, and an anonymous reviewer for constructive feedback that considerably improved this manuscript.

Appendix A. Supplementary material

Supplementary data related to this article can be found online at http://dx.doi.org/10.1016/j.jsg.2014.09.012.

References

Ábalos, B., 1997. Omphacite fabric variation in the Cabo Ortegal eclogite (NW Spain): relationships with strain symmetry during high-pressure deformation. J. Struct. Geol. 19, 621–637.
Andersen, T.B., Berry, H.N., Lux, D.R., Andresen, A., 1998. The tectonic significance of pre-Scandian $^{40}Ar/^{39}Ar$ phengite cooling ages in the Caledonides of western Norway. J. Geol. Soc. 155, 297–309.
Andersen, T.B., Jamtveit, B., Dewey, J.F., Swensson, E., 1991. Subduction and eduction of continental crust: major mechanism during continent–continent collision and orogenic extensional collapse, a model based on the south Caledonides. Terra Nova 3, 303–310.
Barth, N.C., Hacker, B.R., Seward, G.G.E., Walsh, E.O., Young, D., Johnston, S., 2010. Strain within the ultrahigh-pressure Western Gneiss Region of Norway recorded by quartz CPOs. In: Geological Society, London, Special Publications, vol. 335, pp. 663–685.
Bascou, J., Barruol, G., Vauchez, A., Mainprice, D., Egydio-Silva, M., 2001. EBSD-measured lattice-preferred orientations and seismic properties of eclogites. Tectonophysics 342, 61–80.
Bascou, J., Tommasi, A., Mainprice, D., 2002. Plastic deformation and development of clinopyroxene lattice preferred orientations in eclogites. J. Struct. Geol. 24, 1357–1368.
Behr, W.M., Platt, J.P., 2011. A naturally constrained stress profile through the middle crust in an extensional terrane. Earth Planet. Sci. Lett. 303, 181–192.
Blumenfeld, P., Mainprice, D., Bouchez, J.L., 1986. C-slip in quartz from subsolidus deformed granite. Tectonophysics 127, 97–115.
Boundy, T.M., Fountain, D.M., Austrheim, H., 1992. Structural development and petrofabrics of eclogite facies shear zones, Bergen Arcs, western Norway: implications for deep crustal deformational processes. J. Metamorph. Geol. 10, 127–146.
Braathen, A., Nordgulen, Ø., Osmundsen, P.-T., Andersen, T.B., Solli, A., Roberts, D., 2000. Devonian, orogen-parallel, opposed extension in the Central Norwegian Caledonides. Geology 28, 615–618.
Butler, J.P., Jamieson, R.A., Steenkamp, H.M., Robinson, P., 2012. Discovery of coesite–eclogite from the Nordøyane UHP domain, Western Gneiss Region, Norway: field relations, metamorphic history, and tectonic significance. J. Metamorph. Geol. 31, 147–163.
Carswell, D.A., Brueckner, H.K., Cuthbert, S.J., Mehta, K., O'Brien, P.J., 2003a. The timing of stabilisation and the exhumation rate for ultra-high pressure rocks in the Western Gneiss Region of Norway. J. Metamorph. Geol. 21, 601–612.
Carswell, D., Tucker, R., O'Brien, P., Krogh, T., 2003b. Coesite micro-inclusions and the U/Pb age of zircons from the Hareidland Eclogite in the Western Gneiss Region of Norway. Lithos 67, 181–190.
Cuthbert, S.J., Carswell, D.A., Krogh-Ravna, E.J., Wain, A., 2000. Eclogites and eclogites in the Western Gneiss Region, Norwegian Caledonides. Lithos 52, 165–195.
Dobrzhinetskaya, L.F., Eide, E.A., Larsen, R.B., Sturt, B.A., Trønnes, R.G., Smith, D.C., Taylor, W.R., Psukhova, T.V., 1995. Microdiamond in high-grade metamorphic rocks of the Western Gneiss Region, Norway. Geology 23, 597–600.
Fossen, H., 2010. Extensional tectonics in the North Atlantic Caledonides: a regional view. In: Geological Society, London, Special Publications, vol. 335, pp. 767–793.
Fossen, H., Teyssier, C., Whitney, D.L., 2013. Transtensional folding. J. Struct. Geol. 56, 89–102.

Garbutt, J.M., Teyssier, C., 1991. Prism <c> slip in the quartzites of the Oakhurst Mylonite Belt, California. J. Struct. Geol. 13, 657–666.
Ghent, E.D., Stout, M.Z., 1984. TiO_2 activity in metamorphosed pelitic and basic rocks: principles and applications to metamorphism in southeastern Canadian Cordillera. Contrib. Mineral. Petrol. 86, 248–255.
Godard, G., van Roermund, H.L.M., 1995. Deformation-induced clinopyroxene fabrics from eclogites. J. Struct. Geol. 17, 1425–1443.
Griffin, W.L., Brueckner, H.K., 1985. REE, Rb–Sr and Sm–Nd studies of Norwegian eclogites. Chem. Geol. 52, 249–271.
Hacker, B.R., 2007. Ascent of the ultrahigh-pressure Western Gneiss Region, Norway. In: Cloos, M., Carlson, W.D., Gilbert, M.C., Liou, J.G., Sorensen, S.S. (Eds.), Convergent Margin Terranes and Associated Regions: a Tribute to W.G. Ernst, pp. 171–184.
Hacker, B.R., Andersen, T.B., Johnston, S., Kylander-Clark, A.R.C., Peterman, E.M., Walsh, E.O., Young, D., 2010. High-temperature deformation during continental-margin subduction and exhumation: the ultrahigh-pressure Western Gneiss Region of Norway. Tectonophysics 480, 149–171.
Helmstaedt, H., Anderson, O.L., Gavasci, A.T., 1972. Petrofabric studies of eclogite, spinel-websterite, and spinel-lherzolite xenoliths from kimberlite-bearing breccia pipes in southeastern Utah and northeastern Arizona. J. Geophys. Res. 77, 4350–4364.
Hirth, G., Tullis, J., 1992. Dislocation creep regimes in quartz aggregates. J. Struct. Geol. 14, 145–159.
Huang, R., Audétat, A., 2012. The titanium-in-quartz (Ti-in-quartz) thermobarometer: a critical examination and re-calibration. Geochim. Cosmochim. Acta 84, 75–89.
Johnston, S., Hacker, B.R., Ducea, M.N., 2007. Exhumation of ultrahigh-pressure rocks beneath the Hornelen segment of the Nordfjord-Sogn Detachment Zone, western Norway. Geol. Soc. Am. Bull. 119, 1232–1248.
Krabbendam, M., Dewey, J.F., 1998. Exhumation of UHP rocks by transtension in the Western Gneiss Region, Scandinavian Caledonides. In: Geological Society, London, Special Publications, vol. 135, pp. 159–181.
Labrousse, L., Jolivet, L., Andersen, T.B., Agard, P., Hébert, R., Maluski, H., Schärer, U., 2004. Pressure–temperature–time deformation history of the exhumation of ultra-high pressure rocks in the Western Gneiss Region, Norway. In: Whitney, D.L., Teyssier, C., Siddoway, C.S. (Eds.), Gneiss Domes in Orogeny, Geological Society of America Special Paper, vol. 380, pp. 155–183.
Mainprice, D., Bouchez, J.-L., Bluemenfeld, P., Tubià, J.M., 1986. Dominant *c* slip in naturally deformed quartz: implications for dramatic plastic softening at high temperature. Geology 14, 819–822.
Mauler, A., Bystricky, M., Kunze, K., Mackwell, S., 2000. Microstructures and lattice preferred orientations in experimentally deformed clinopyroxene aggregates. J. Struct. Geol. 22, 1633–1648.
Müller, A., Wiedenbeck, M., van den Kerkhof, A.M., Kronz, A., Simon, K., 2003. Trace elements in quartz – a combined electron microprobe, secondary ion mass spectrometry, laser-ablation ICP–MS, and cathodoluminescence study. Eur. J. Mineral. 15, 747–763.
Nachlas, W.O., Whitney, D.L., Teyssier, C., Bagley, B., Mulch, A., 2014. Titanium concentration in quartz as a record of multiple deformation mechanisms in an extensional shear zone. Geochem. Geophys. Geosyst. 15, 1374–1397.
Norton, M.G., 1986. Late Caledonide extension in Western Norway – a response to extreme crustal thickening. Tectonics 5, 195–204.
Norton, M.G., 1987. The Nordfjord-Sogn detachment, Western Norway. Nor. Geol. Tidsskr. 67, 93–106.
Passchier, C.W., Simpson, C., 1986. Porphyroclast systems as kinematic indicators. J. Struct. Geol. 8, 831–843.
Root, D.B., Hacker, B.R., Gans, P.B., Ducea, M.N., Eide, E.A., Mosenfelder, J.L., 2005. Discrete ultrahigh-pressure domains in the Western Gneiss Region, Norway: implications for formation and exhumation. J. Metamorph. Geol. 23, 45–61.
Root, D.B., Hacker, B.R., Mattinson, J.M., Wooden, J.L., 2004. Zircon geochronology and ca. 400 Ma exhumation of Norwegian ultrahigh-pressure rocks: an ion microprobe and chemical abrasion study. Earth Planet. Sci. Lett. 228, 325–341.
Smith, D.C., 1984. Coesite in clinopyroxene in the Caledonides and its implications for geodynamics. Nature 310, 641–644.
Smith, D.C., Godard, G., 2013. A Raman spectroscopic study of diamond and disordered sp^3-carbon in the coesite-bearing Straumen Eclogite Pod, Norway. J. Metamorph. Geol. 31, 19–33.
Smyth, J.R., 1977. Quartz pseudomorphs after coesite. Am. Mineral. 65, 1185–1191.
Stipp, M., Stünitz, H., Heilbronner, R., Schmid, S., 2002. The eastern Tonale fault zone: a 'natural laboratory' for crystal plastic deformation of quartz over a temperature range from 250 to 700 °C. J. Struct. Geol. 24, 1861–1884.
Terry, M.P., Robinson, P., 2003. Evolution of amphibolite-facies structural features and boundary conditions for deformation during exhumation of high- and ultrahigh-pressure rocks, Nordøyane, Western Gneiss Region, Norway. Tectonics 22.
Terry, M.P., Robinson, P.R., Krogh Ravna, E.J., 2000. Kyanite eclogite thermobarometry and evidence for thrusting of UHP over HP metamorphic rocks, Nordøyane, Western Gneiss Region, Norway. Am. Mineral. 85, 1637–1650.
Thomas, J.B., Spear, F.S., Webb, L.E., 2012. Experimental study of titanium-in-coesite solubility. In: Abstract V33C-2885 Presented at 2012 Fall Meeting. American Geophysical Union, San Francisco, California, 3–7 Dec.
Thomas, J.B., Watson, E.B., Spear, F.S., Shemella, P.T., Nayak, S.K., Lanzirotti, A., 2010. TitaniQ under pressure: the effect of pressure and temperature on the solubility of Ti in quartz. Contrib. Mineral. Petrol. 160, 743–759.
Tullis, J., 1977. Preferred orientation of quartz produced by slip during plane strain. Tectonophysics 39, 87–102.
Vrijmoed, J.C., van Roermund, H.L.M., Davies, G.R., 2006. Evidence for diamond-grade ultra-high pressure metamorphism and fluid interaction in the Svartberget Fe–Ti garnet peridotite–websterite body, Western Gneiss Region, Norway. Mineral. Petrol. 88, 381–405.
Wain, A., 1997. New evidence for coesite in eclogite and gneisses: defining an ultrahigh-pressure province in the Western Gneiss Region of Norway. Geology 25, 927–930.
Wain, A., Waters, D., Jephcoat, A., Olijyink, H., 2000. The high-pressure to ultrahigh-pressure eclogite transition in the Western Gneiss Region, Norway. Eur. J. Mineral. 12, 667–687.
Wark, D.A., Watson, E.B., 2006. TitaniQ: a titanium-in-quartz geothermometer. Contrib. Mineral. Petrol. 152, 743–754.
Whitney, D.L., Evans, B.W., 2010. Abbreviations for names of rock-forming minerals. Am. Mineral. 95, 185–187.
Young, D.J., Hacker, B.R., Andersen, T.B., Gans, P.B., 2011. Structure and $^{40}Ar/^{39}Ar$ thermochronology of an ultrahigh-pressure transition in western Norway. J. Geol. Soc. 168, 887–898.
Zhang, J., Green, H.W., 2007. On the deformation of UHP eclogite: from laboratory to nature. Int. Geol. Rev. 29, 487–508.
Zhang, J., Green, H.W., Bozhilov, K.N., 2006. Rheology of omphacite at high temperature and pressure and significance of its lattice preferred orientations. Earth Planet. Sci. Lett. 246, 432–443.
Zhang, J.F., Shi, F., Xu, H.J., Wang, L., Feng, S.Y., Liu, W.L., Wang, Y.F., Green, H.W., 2013. Petrofabric and strength of SiO_2 near the quartz–coesite phase boundary. J. Metamorph. Geol. 31, 83–92.
Zheng, Y.-F., 2012. Metamorphic chemical geodynamics in continental subduction zones. Chem. Geol. 328, 5–48.